Density functional studies of the defect-induced electronic structure modifications in bilayer boronitrene

A M Ukpong[1,*] and N Chetty[1,2]
[1] Department of Physics, University of Pretoria, Hatfield 0002, South Africa
[2] National Institute for Theoretical Physics, Johannesburg 2000, South Africa

E-mail: aniekan.ukpong@up.ac.za

Abstract. The van der Waals interaction-corrected density functional theory is used in this study to investigate the formation, energetic stability, and inter-layer cohesion in bilayer hexagonal boronitrene. The effect of inter-layer separation on the electronic structure is systematically investigated. The formation and energetic stability of intrinsic defects are also investigated at the equilibrium inter-layer separation. It is found that nonstoichiometric defects, and their complexes, that induce excess nitrogen or excess boron, in each case, are relatively more stable in the atmosphere that corresponds to the excess atomic species. The modifications of the electronic structure due to formation of complexes are also investigated. It is shown that van der Waals density functional theory gives an improved description of the cohesive properties but not the electronic structure in bilayer boronitrene compared to other functionals. We identify energetically favourable topological defects that retain the energy gap in the electronic structure, and discuss their implications for band gap engineering in low-*n* layer boronitrene insulators. The relative strengths and weaknesses of the functionals in predicting the properties of bilayer boronitrene are also discussed.

1. Introduction

The hexagonal boron nitride (*h*-BN) monolayer has attracted sustained interests in recent times as the boron nitride analogue of graphene. Its stability as a freestanding monolayer and as a coupled system of few single layers (FSLs) [1] offers a unique opportunity for the exploration of the rich physics associated with graphene. Because *h*-BN has a wide band gap and no lattice mismatch with graphene, thin *h*-BN layers are useful in microelectronics as thin top-dielectric to gate graphene [2], inert substrates (or spacers) and scaffolds for graphene support [3,4]. For instance, the use of FSLs of *h*-BN in quantum-well heterostructures has been reported to improve the electronic quality of heterojunction devices compared to the use of highly-oriented pyrolytic boron nitride [5]. Nevertheless, the fewer number of experimental studies on *h*-BN nanosheets indicates that low-*n* layer *h*-BN is not fully explored compared to graphene. This situation arises because the synthesis of BN-based nanostructures is significantly more challenging than carbon based nanostructures because the well-developed methods for graphene synthesis are not always suitable for boronitrene synthesis [6]. Defects may be introduced deliberately to modify the wide band gap during synthesis. Because such

* To whom any correspondence should be addressed.

defects can also occur spontaneously, it is important to understand the influence of defects on the electronic structure of low-*n* layers of *h*-BN. The dependence of the formation energy on growth conditions is also relevant for the stability of defective *h*-BN layers. This paper focuses on the modifications of the electronic structure in bilayer *h*-BN due to intrinsic defects. Defects that are capable of retaining the gap between the valence and conduction bands are identified.

2. Computational Methods

First principles calculations were performed based on density functional theory (DFT) as implemented in Quantum ESPRESSO [7]. The calculations were initially performed using the local density and generalized gradient approximations (LDA [8] and GGA [9]) to the exchange-correlation (XC) interactions. The GGA parameterization of Perdew, Burke, and Ernzerhof (GGA-PBE) [9] was used. Because of dispersive interactions [10] between coupled *h*-BN layers, we have also used the van der Waals interaction-corrected density functional (vdW-DF) to determine the ground state properties [11,12]. The interaction between valence electrons and ionic cores were described using the projector-augmented wave (PAW) potentials [13,14]. The kinetic energy cut-off of 500 eV was used for the plane wave expansion, and the electronic energy was converged to within 10^{-7} eV. The Monkhorst-Pack scheme was used to sample the Brillouin zone [15]. The electronic states were populated in accordance with the Fermi distribution function, with a smearing parameter of 0.2 eV. The atomic forces were calculated using the Hellman-Feynman theorem, and the atomic positions were relaxed until the forces were reduced to less than 0.03 eVÅ^{-1}. Convergence tests on the total energy differences were performed on the 4-atom unit cell with respect to k-points. It was concluded that the 12×12×1 sampling of the Brillouin zone was sufficiently converged. The total energy of the pristine bilayer was optimized with respect to the lattice parameter for the three XC functionals. The vacuum height was optimised to 15 Å to avoid spurious interlayer interactions.

3. Results and Discussion

Bilayer *h*-BN exists in five stacking sequences because the basis atoms of the top and bottom layer are dissimilar. Two of the sequences (*i.e.* AA and AA') give the simple stacking conformation, while the remainder (i.e. by A'B, AB' and AB) give the Bernal AB stacking conformation [16]. Table 1 shows the effect of stacking sequence on vdW-DF optimised properties of bilayer *h*-BN. The difference in total energy per unit cell δE is evaluated with respect to the AB-stacked structure because its total energy is lowest. From Table 1, the total energy of the AA'-stacked *h*-BN bilayer is 3.4 meV and 10.75 meV lower than the AB' and A'B-stacked bilayer *h*-BN structures respectively. We therefore conclude that the most unstable form of pristine *h*-BN bilayer is stacked in the AA sequence.

Table 1. Effect of stacking sequence on properties of bilayer h-BN. The last column indicates the pair of atoms used to determine the interlayer distance *d*.

Stacking	δE (meV/cell)	Δ_c (eV)	Δ_v (eV)	m^*	$l_{B\text{-}N}$ (Å)	d (Å)	Atom
A'B	36.87	0.77	1.353	0.36	1.451	3.79	N-N
AB'	29.52	0.96	1.210	0.29	1.443	3.36	B-B
AB	0.00	1.46	1.165	0.19	1.452	3.32	B-N
AA'	26.12	0.87	1.305	0.32	1.452	3.55	B-N
AA	37.28	0.58	1.208	0.48	1.452	3.74	B-B

The vdW-DF, GGA-PBE and LDA band structure of the AB-stacked pristine *h*-BN bilayer is shown in Figure 1. The functionals yield similar electronic structure and show non-degenerate π-bands at point K. However, the GGA and vdW-DF give small energy shifts (see Table 2), whereas the LDA gives a larger shift between the two top-most lying π-bands. The difference in the positions of the GGA-PBE and vdW-DF Fermi levels (indicated with dashed horizontal lines in Fig. 1) is small. This indicates that vdW-DF does not necessarily give an improved description of the electronic structure in

bilayer *h*-BN. Although the vdW-DF band gap (4.76 eV) is significantly higher than the LDA band gap, the vdW-DF band gap is 0.74 eV lower than the experimental value of 5.50 eV [17]. By contrast, the deviation of the GGA-PBE band gap (5.35 eV) from the experimental band gap is less than 3%. We therefore conclude that vdW-DF does not provide an improved description of the electronic structure in the bilayer *h*-BN. Instead, GGA-PBE gives a better estimate of the experimental band gap.

Table 1 also shows the vdW-DF conduction and valence band widths. These were evaluated as differences, $\Delta = E$(K-point) – E(Γ-point), relative to the Fermi energy for the lowest unoccupied (Δ_c) and highest occupied (Δ_v) π-bands, respectively. From Δ_c (see Table 1), the predicted effective mass m^* is lowest (0.19) in the AB-stacked sequence and highest (0.48) in the AA-stacked sequence. The group velocity v_g for electron drift in the conduction band along the Γ→K direction of the Brillouin zone also shows that electrons attain their highest speed (54×10^6 m/s) and lowest speed (21×10^6 m/s) in the AA- and AB-stacked structures respectively. In the valence band however, electrons in the AB-stacked structure have the highest speed (27×10^6 m/s) compared to the lowest speed (23×10^6 m/s) in the A'B-stacked structure.

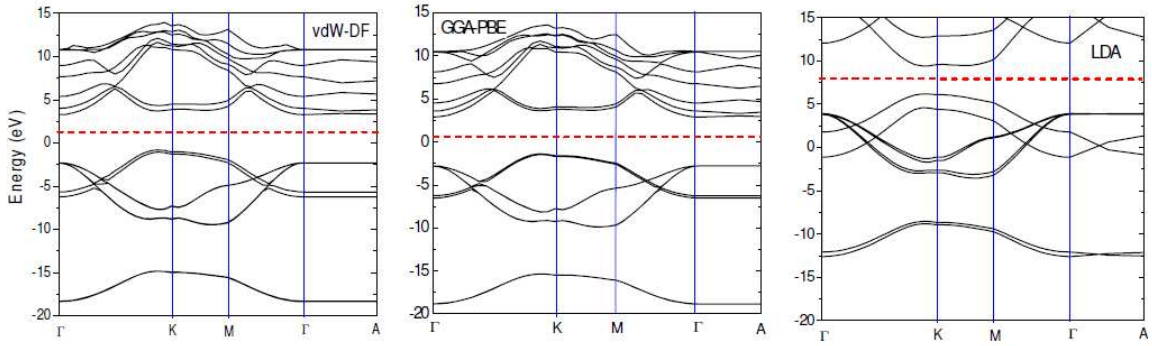

Figure 1. Band structure of pristine AB-stacked bilayer boronitrene at equilibrium interlayer spacing.

Table 2. Stereo-electronic properties of pristine bilayer hexagonal boronitrene.

Functional	$l_{B\text{-}N}$ (Å)	d_0(Å)	E_{coh} (eV/atom)	Electronic properties at point-K	
				Band gap (eV)	π-band shift (eV)
vdW-DF	1.442	3.32	-0.40	4.76	0.268
GGA-PBE	1.452	4.28	-0.33	5.35	0.094
LDA	1.447	3.78	-0.26	3.41	1.587

The lattice parameter is 2.50 Å, 2.52 Å, and 2.51 Å after optimisation with vdW-DF, GGA-PBE, and LDA functional, respectively. These values compare favourably with the experimental value of 2.50 Å [18,19], and with the value of 2.51 Å obtained from DFT calculations for monolayer *h*-BN [20,21]. In addition, the cohesive energy per atom was determined using the expression $E_{coh} = \left(E_{\text{pair}}^{\text{BN}} - E^{\text{B}} - E^{\text{N}}\right)/\text{N}$, where $E_{\text{pair}}^{\text{BN}}$ is the total energy per pair of B-N atoms in the equilibrium structure. The terms E^{B} and E^{N} denote the total energies of the free B and N atoms respectively. The cohesive energy of -14.6 eV (vdW-DF), -11.88 eV (GGA-PBE) and -9.36 eV (LDA) was obtained for pristine *h*-BN bilayer. Table 2 shows the stereo-electronic properties of *h*-BN bilayer from the three XC functional. The vdW-DF predicts the strongest structural cohesion compared to GGA-PBE and LDA. The strong binding from vdW-DF is also seen in the short interlayer separation (3.32 Å) compared to 4.28 Å obtained from GGA-PBE. The interlayer distance is ~0.9% shorter than the experimental interlayer distance (3.35 Å) expected in bilayer *h*-BN. These indicate that dispersive interactions play a nontrivial role in the determination of the cohesive properties of bilayer *h*-BN.

One way of obtaining a defective *h*-BN bilayer is through the application of uniaxial strain. The strain, in this case, is applied along the *c*-axis (*i.e.* normal to the stacking direction). Figure 2 shows the effect of uniaxial strain on the electronic band edges. The top (and bottom) panels in Fig. 2

correspond to decreasing (and increasing) interlayer distances respectively. We find that the shift in energy between the two top-most lying π-bands at points *K* (valence band) and *K*' (conduction band) increases as the interlayer separation is reduced from the value in the optimised structure. The corresponding positions of the HOMO and LUMO states also respond to applied uniaxial compression, and give rise to decreased band gaps. It is noted that the widest band gap occurs at the equilibrium interlayer separation of 3.32 Å. Taken together, the increase in band gap with increasing interlayer distances up to the equilibrium interlayer separation is ascribed to the strain-induced removal of the π-band degeneracy at point *K* - suggesting the possibility of tuning the band gap in bilayer *h*-BN by strain engineering. The lower panels of Fig. 2 show that application of uniaxial tensile strain does not shift the energy levels of the π-bands. Thus, no change is observed in the band gap, although the application of uniaxial tensile strain removes the degeneracy of the bands.

Our vdW-DF band structure calculations show increased in-plane band distortions as interlayer distance is decreased. These indicate that electrons acquire substantially higher speeds within the plane. Out-of-plane band distortions, i.e. along Γ→A, are minimal even at very small interlayer distances for which the van der Waals interactions are strong. At large interlayer distances, therefore, we cannot attribute the observed crossings in the three lower conduction bands to enhanced out-of-plane electron mobility due to substantially weakened van der Waals interactions. In addition, because the band dispersions are correctly described within the plane of the bilayer (i.e. Γ→M→K→Γ) at short interlayer distances, we attribute the non-monotonous variation of the Γ-point energy, observed at 6, 7 and 8 Å, to the decoupling of the bilayer at large distances.

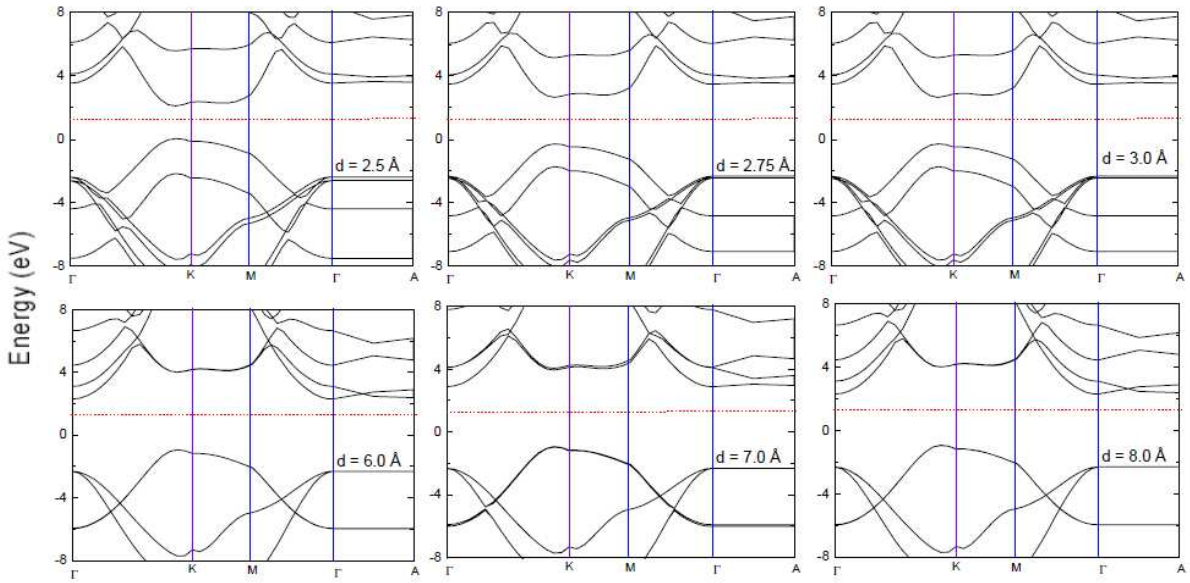

Figure 2. Effect of *c*-axis compressive (top panels) and tensile (bottom panels) strain on the band edges for varying interlayer separations. The Fermi level is denoted with horizontal lines.

Reduced band gaps can also obtained by breaking the symmetry of the ordered honeycomb structure. However, only the intrinsic defects, shown in Fig. 3 (a)-(i), are considered in the present study. The total energy was also converged with respect to supercell size. The difference Δ*E* between the total energies of the defect-free and defective structures of size 3×3 and 4×4 converges to 31 meV for V_B+V_B complex. Because this configuration has the most extended open-volume, we conclude that the total energy of the defective system is well converged. A 3×3 supercell with lattice parameter $a = b$ = 7.53 Å was used in the calculations reported here. In the present study, the local structure of the complexes is not constrained to nearest neighbour positions unlike in our previous studies of defects in monolayer *h*-BN [22]. Stoichiometric defects that can form on one layer, or on both layers, of the

bilayer structure are denoted with an asterisk. We note that their total energies are lower when they form on one layer compared to both layers. When formed in one layer in each case, the total energy of the V_N+V_B complex is 1.47 eV lower while the Stone-Wales defect is 8.71 eV lower than in both layers. The formation of nonstoichiometric complexes (as point defects on both layers) give total energies that are at least 20.41 eV lower than when the defects are formed on only one layer.

Fig. 3(j) shows the formation energy of neutral defects as a function of changes in chemical potential, $\Delta\mu$. The formation energies are constrained to vary within the interval, $-\Delta H_f \le \Delta\mu \le +\Delta H_f$, fixed by the formation energy ΔH_f of the pristine bilayer. We calculated ΔH_f using $\Delta H_f = -(\mu_{BN} - \mu_B^{bulk} - \mu_N^{bulk})$, and obtained the value of -2.58 eV in good agreement with the experimental value of -2.60 ± 0.02 eV [23]. The boron-rich and nitrogen-rich conditions correspond to limits $+\Delta H_f$ and $-\Delta H_f$ respectively. The formation energy of nonstoichiometric defects is dependent on $\Delta\mu$, as expected. The V_N and its complexes are more stable than the V_B and its complexes in B-rich condition, and vice versa. The creation of the double N (or B) antisite complex at B (or N) sites on both layers, or on nearest neighbour sites on one of the layers presents the lowest formation energy in N-rich and B-rich conditions, respectively. This trend is also seen in the double antisite complexes of B (N_B+N_B) and N (B_N+B_N) when they are created on both top and bottom layers. We find that nonstoichiometric complexes that induce excess nitrogen or boron, in each case, are relatively more stable in the growth condition that is rich in the excess atomic species.

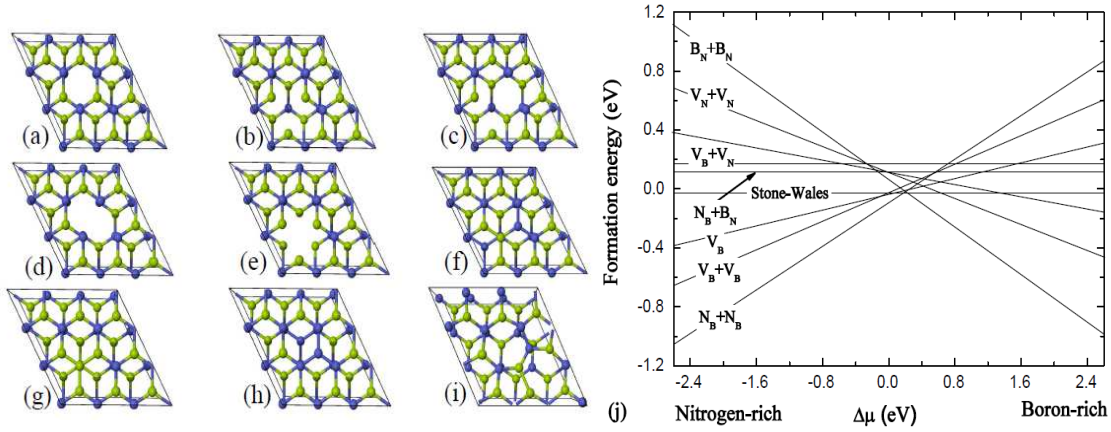

Figure 3. (a) V_B, (b) V_N, (c) V_N+V_B(*), (d) V_B+V_B, (e) V_N+V_N, (f) N_B+N_B, (g) B_N+B_N, (h) N_B+N_B, (i) Stone-Wales (SW) defect (*), and (j) their energies of formation as a function of changes in atomic chemical potential.

The electronic density of states (EDOS) gives an estimate of how closely packed the energy levels are distributed within an energy interval. Because the band structure is modified by defects, the defect states are required to form *e*-resonances with the top of the valence band (VB) or bottom of the conduction band (CB) in order to maintain the semiconducting band gap. When a defect state forms an *s*-resonance at the Fermi level, it eliminates the band gap by bridging the VB and CB. This induces metallic transport properties. We find that boron and nitrogen vacancies and their complexes introduce *s*-resonance to the Fermi level in bilayer *h*-BN. Figure 4 shows the EDOS of the V_B+V_N complex and the Stone-Wales (SW) defect. Both defects are formed on one layer. The Fermi levels correspond to -0.38 eV (V_B+V_N) and 0.31 eV (SW) respectively. All other defects introduce defect states that form *s*-resonances with the Fermi level. In the monolayer for instance, replacing a boron atom with the carbon impurity (C_B) leads to the highest stability [22,23]. More importantly, because the smallest band gap is obtained in C_B [24], we suggest the possibility of further reducing the band gaps in V_B+V_N and SW layers by impurity adsorption.

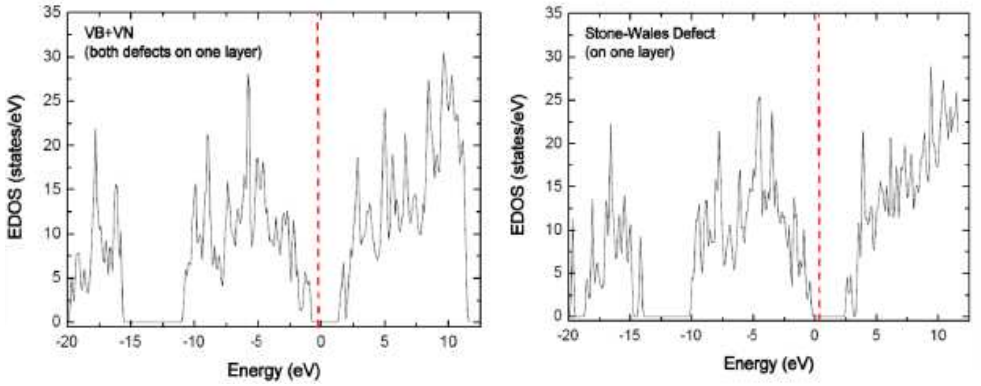

Figure 4. Electronic density of states in V_B+V_N complex and the Stone-Wales defect.

4. Conclusion

A comparative density functional study of the ground state properties of bilayer *h*-BN has been presented. We conclude that the vdW-DF gives a better description of the cohesive properties while the GGA-PBE gives the widest band gap in agreement with experiments. Using the vdW-DF, it is shown that band gap modification in the *h*-BN bilayer is achievable by application of uniaxial compressive strain, and by introduction of defects. Only the stoichiometric V_B+V_N complex and the Stone-Wales defect are able to preserve the band gap. Both defects present their lowest formation energies when they form on either the top or bottom layer of the coupled *h*-BN bilayer.

Acknowledgements

This work was supported by the University of Pretoria under E2020 Project No. 5. NC is grateful to the National Institute for Theoretical Physics for support.

References

[1] Gorbachev R V, Riaz I, Nair R R, *et al.* 2011 *Small* 7 465
[2] Young A F, Dean C R, Meric I, *et al.* 2010 *arXiv:1004.5556*
[3] Dean C R, Young A F, Meric I, *et al.* 2010 *Nature Nanotech.* **5** 722
[4] Lee C, Li Q, Kalb W, *et al.* 2010 *Science* **328** 76
[5] Ponomarenko L A, Yang R, Mohiuddin T M, *et al.* 2009 *Phys. Rev. Lett.* **102** 206603
[6] Golberg D, Bando Y, Huang Y, *et al.* 2010 *ACSNANO* **4** 2979
[7] Giannozzi P *et al.* 2009 *J. Phys Condens. Matter* **21** 395502
[8] Perdew J P and Zunger A 1981 *Phys. Rev.* B **23** 5048
[9] Perdew J P, Burke K and Ernzerhof M 1996 *Phys. Rev. Lett.* **77** 18
[10] Barone V, Casarin M, Forrer D, *et al.* 2009 *J. Comput. Chem.* **30** 934
[11] Dion M, Rydberg H, Schroder E, *et al.* 2004 *Phys. Rev. Lett.* **92** 246401
[12] Roman-Perez G and Soler J M 2009 *Phys. Rev. Lett***. 103** 096102
[13] Kresse G and Joubert D 1999 *Phys. Rev.* B **59** 1758
[14] Blöchl P E 1994 *Phys. Rev.* B **50** 17953
[15] Monkhorst H J and Pack J D 1976 *Phys. Rev.* B **13** 5188
[16] Ribeiro R M and Peres N M R 2011 *Phys. Rev.* B **83** 235312
[17] Song L, Ci L, Lu H, *et al.* 2010 *Nano Lett.* **10** 3209
[18] Meyer J C, Chuvilin A, Algara-Siller G, *et al.* 2009 *Nano Lett.* **9** 2683
[19] Li J, Gui G and Zhong J 2008 *J. App. Phys.* **104** 094311
[20] Azevedo S, Kaschny J R, de Castilho C M C, *et al.* 2009 *Eur. Phys. J.* B **67** 507
[21] Solozenko V L, Will G and Elf F 1995 *Solid State Commun.* **96** 1
[22] Ngwenya T B, Ukpong A M and Chetty N 2011 *Phys. Rev.* B **84** 245425
[23] Wise S S, Margrave J L, Feder H M, Hubbard W N 1966 *J. Phys. Chem.* **70** 7
[24] Jin C, Lin F, Suenaga K and Iijima S 2009 *Phys. Rev. Lett.* **102** 195505